

# GUIDANCE SOLUTIONS FOR SPACECRAFT PLANAR REPHASING AND RENDEZVOUS USING INPUT SHAPING CONTROL

M. Lawn,<sup>\*</sup> G. Di Mauro,<sup>†</sup> and R. Bevilacqua<sup>‡</sup>

Small satellites formation flying has been attracting growing interest. While economical to design and to launch, they have limited computational capability and propellant capacity. Thrusters must generally have a small form factor and use minimal propellant, often operating only in on/off configurations and with a few set force magnitudes. Therefore, efficient relative orbit control techniques must be developed to satisfy low-thrust constraints without reducing performance accuracy or straining the limited computational power of the small on-board systems. This paper presents analytical guidance solutions for orbital planar spacecraft rephasing and rendezvous using in-plane continuous low-thrust profiles derived from input shaping theory.

## INTRODUCTION

The use of small satellites flying in close proximity is increasing at a rapid pace for many types of missions, including space science, Earth observation and remote sensing, Earth science, and technology demonstration.<sup>1</sup> Thanks in part to the growth in popularity of the CubeSat standard and related components and technologies, small satellites (herein defined as those satellites with wet mass less than 500 kg) are generally more economical to design and launch than large satellites.<sup>2,3</sup> Several small satellites flying in formation can perform the tasks assigned to a single large satellite, while providing increased adaptability, versatility, and robustness. A small satellite formation can be reconfigured as mission directives change or to take on a pattern better suited to its task. It may be adjusted to compensate for a single malfunctioning vehicle without necessitating a mission abort. The formation could even be separated and viable individual satellites reassigned to other missions at the end of the original mission lifetime.

However, small satellites present their own variety of design challenges, especially in the areas of guidance, navigation, and control (GNC). The primary obstacle is limited onboard storage space, which restricts both available power and propulsion system complexity. High performance space-qualified on-board computers require high power to work, thus small spacecraft generally have limited computing capability. Moreover, in order to meet the physical dimension constraints, they are typically equipped with small thrusters providing low thrust and operating only in on/off configurations with a few set force magnitudes. In addition, some satellite configurations require a level of on-board autonomy to guarantee highly accurate performance and an efficient and prompt response to contingencies. This implies that GNC solutions must be computed on-board to meet mission requirements.

---

<sup>\*</sup> Graduate Student, Department of Mechanical & Aerospace Engineering, ADAMUS Laboratory, University of Florida, 939 Sweetwater Dr., Gainesville, FL 32611 – 6250.

<sup>†</sup> PostDoc Associate, Department of Mechanical & Aerospace Engineering, ADAMUS Laboratory, University of Florida, 939 Sweetwater Dr., Gainesville, FL 32611 – 6250.

<sup>‡‡</sup> Associate Professor, Department of Mechanical & Aerospace Engineering, ADAMUS Laboratory, University of Florida, 939 Sweetwater Dr., Gainesville, FL 32611 – 6250.

In light of the above, efficient relative orbit control techniques must be developed to satisfy the low-thrust constraints without reducing performance accuracy or straining the limited computational power of the small on-board systems.

One such method is bang-bang control, filtered via input shaping. Input shaping is a technique consisting of the convolution of a feedforward control signal with a series of delayed impulses. The temporal distribution and magnitudes of these impulses depend on natural frequency and damping of the system respectively.<sup>4</sup> This technique has been extensively examined for vibration suppression of flexible manipulators, and more recently it has been proposed for orbital maneuvering of spacecraft systems.<sup>5</sup> It is worth pointing out that input shaping is not intended to reduce the energy of the system, i.e. it cannot damp the system oscillations completely. However, an appropriate choice of the shaper's parameters enables the modification of the system's oscillatory behavior. In the context of spacecraft relative maneuvering this means that input shaping can be exploited to maneuver the satellite from one equilibrium configuration to another, modifying the periodic relative motion.<sup>6</sup> In this paper, the input shaping method is proposed to compute the guidance solutions to the problems of short-distance planar spacecraft rephasing and rendezvous, when continuous low-thrust is used.

The rest of the paper is organized as follows. In the first section, the spacecraft relative dynamics model and its analytical solution are presented. In the next section two types of shapers, the Zero Vibration shaper and the Zero Vibration Derivative shaper, are introduced and the shaper profiles are described. The subsequent section is dedicated to the derivation of analytical solutions for the final state, center of final relative ellipse, final relative eccentricity, and condition for final orbit equilibrium. Then the guidance trajectories obtained using the shaped thrust profile and spacecraft dynamics model are presented. The final section shows optimization of shaper parameters to obtain a desired relative eccentricity while minimizing control action.

## DYNAMICS MODEL

Unlike the work presented by one of the authors of this paper in (Reference 5), this study uses a more accurate relative dynamics model to derive the analytical guidance law through the input shaping technique. This model, developed by Schweighart and Sedwick (SS), includes the effects of the second order perturbative term of the Earth's geopotential by adding the linearized  $J_2$  force as a forcing function.<sup>7</sup> This leads to the following set of linearized, constant-coefficient differential equations of relative motion<sup>8</sup>

$$\begin{aligned} \ddot{x} - 2\bar{m}\dot{y} - (4\bar{m}^2 - \bar{n}^2)x &= u_x \\ \dot{y} + 2\bar{m}\dot{x} &= u_y \end{aligned} \quad (1)$$

$$\ddot{z} + (2\bar{m}^2 - \bar{n}^2)z = u_z \quad (2)$$

where

$$k_{j_2} = \frac{3}{8}J_2 \frac{R_e^2}{r_{ref}^2} (1 + 3 \cos(2i_{ref})), \quad \bar{m} = n_{ref} \sqrt{1 + k_{j_2}}, \quad \bar{n} = n_{ref} \sqrt{1 - k_{j_2}}, \quad (3)$$

with  $J_2 = 0.0019827$  and  $R_e$  the mean Earth radius. The above equations are expressed in the local vertical, local horizontal (LVLH) reference frame initially centered in the chief's center of mass and moving on a circular orbit of radius  $r_{ref}$  and inclination  $i_{ref}$  with the rotational rate  $n_{ref}$ .  $x$  points radially away from the planet to the reference satellite,  $z$  is the direction of the orbit's angular momentum, and  $y$  completes the right-handed ortho-normal basis. Although accurately describing the relative motion under the effect of  $J_2$  potential, the SS equations can still be solved analytically and then ease the derivation of the analytical guidance solution.

From Eqs. (1) and (2) it is clear that the motion in the  $z$  direction is decoupled from the motion in the  $x$  and  $y$  directions. For this reason, we consider only the in-plane ( $x$ - $y$ ) dynamics in this study. The analytical solution to the SS equations for planar motion is the following:

$$\begin{pmatrix} \dot{x} \\ \dot{y} \\ \ddot{x} \\ \ddot{y} \end{pmatrix} = \Phi(t, t_0) \begin{pmatrix} x_0 \\ y_0 \\ \dot{x}_0 \\ \dot{y}_0 \end{pmatrix} + \Psi(t) \begin{pmatrix} u_x \\ u_y \end{pmatrix}$$

$$\Phi(t, t_0) = \begin{bmatrix} \frac{a^2}{\bar{n}^2} - \frac{b}{\bar{n}^2} \cos(\bar{n}t) & 0 & \frac{\sin(\bar{n}t)}{\bar{n}} & \frac{a}{\bar{n}^2} (1 - \cos(\bar{n}t)) \\ -\frac{ab}{\bar{n}^2} \left( dt - \frac{\sin(\bar{n}t)}{\bar{n}} \right) & 1 & -\frac{a}{\bar{n}^2} (1 - \cos(\bar{n}t)) & \frac{a^2}{\bar{n}^3} \sin(\bar{n}t) - \frac{b}{\bar{n}^2} dt \\ b \left( \frac{\sin(\bar{n}t)}{\bar{n}} \right) & 0 & \cos(\bar{n}t) & \frac{a}{\bar{n}} \sin(\bar{n}t) \\ -\frac{ab}{\bar{n}^2} (1 - \cos(\bar{n}t)) & 0 & -\frac{a}{\bar{n}} \sin(\bar{n}t) & \frac{a^2}{\bar{n}^2} \cos(\bar{n}t) - \frac{b}{\bar{n}^2} \end{bmatrix} \quad (4)$$

$$\Psi(t) = \begin{bmatrix} \frac{1}{\bar{n}^2} (1 - \cos(\bar{n}t)) & \frac{a}{\bar{n}^2} \left( dt - \frac{\sin(\bar{n}t)}{\bar{n}} \right) \\ -\frac{a}{\bar{n}^2} \left( dt - \frac{\sin(\bar{n}t)}{\bar{n}} \right) & \frac{(\bar{n}^2 + b)}{\bar{n}^4} (1 - \cos(\bar{n}t)) - \frac{b}{\bar{n}^2} \frac{dt^2}{2} \\ \frac{\sin(\bar{n}t)}{\bar{n}} & \frac{a}{\bar{n}^2} (1 - \cos(\bar{n}t)) \\ -\frac{a}{\bar{n}^2} (1 - \cos(\bar{n}t)) & \frac{\sin(\bar{n}t)}{\bar{n}} + \frac{b}{\bar{n}^2} \left( \frac{\sin(\bar{n}t)}{\bar{n}} - dt \right) \end{bmatrix}$$

where

$$a = 2\bar{m} \quad b = 5\bar{m}^2 - 2n^2 \quad dt = t - t_0 \quad (5)$$

## INPUT SHAPER BASICS

The main idea of the input shaping method is based on the convolution of the command signal with a sequence of Dirac impulses. These impulses have to be applied in specified moments of time and with specified amplitude in order to nullify the residual vibrations of the system (Reference 4).

This study investigates two classes of shapers, namely the Zero Vibration (ZV) shaper and the Zero Vibration Derivative (ZVD) shaper. They are used to shape a bang-bang thrust profile of amplitude  $\bar{u}$ .

### Zero Vibration Shaper

The ZV shaper is probably the simplest input shaper.<sup>9</sup> It is designed to filter an incoming signal such that the system driven by the new shaped command will not have vibration arising from the frequency filtered out by the ZV shaper. It consists of two impulses whose temporal distribution and magnitudes are

$$T = [t_1, t_2] = [0 \quad \Delta t] \quad (6)$$

$$A = [A_1, A_2] = \left[ \frac{\zeta}{\zeta + 1}, \frac{1}{\zeta + 1} \right] \quad (7)$$

where

$$\zeta = e^{\frac{\zeta\pi}{\sqrt{1-\zeta^2}}} \quad (8)$$

with  $\zeta$  the damping ratio of the system. The values  $T$  and  $A$  are the time by which each impulse is delayed and its corresponding amplitude. Note that when  $\Delta t = \pi/\omega_d$ , where  $\omega_d$  indicates the damped natural frequency of the system, the command shaper described by Eqs. (6)-(8) will suppress the system residual vibrations.

For the purpose of deriving a control profile for the in-plane deputy maneuvering, the aforementioned shaper can be used to shape a bang-bang continuous command of amplitude  $\bar{u}$ . In further detail, let us assume that the deputy provides a continuous thrust  $\mathbf{U} = [u\sin(\alpha), u\cos(\alpha)]^T$ , where  $u$  is the shaped bang-bang command and  $\alpha$  the angle between the in-plane projection of control vector and the y-axis of LVLH reference frame. Then, the shaped control command can be formulated as follows:

$$\mathbf{u} = A_1 f_{t1} + A_2 f_{t2} \quad (9)$$

where

$$f_{t1} = \begin{cases} 0 & t > t^* \\ \bar{u} \operatorname{sign}(\bar{y}_d - y_0) & t < t^*/2 \\ -\bar{u} \operatorname{sign}(\bar{y}_d - y_0) & t^*/2 < t < t^* \end{cases} \quad (10)$$

$$f_{t2} = f_{t1}(t - \Delta t),$$

where  $y_0$  is the initial relative along-track position,  $\bar{y}_d$  is the desired along-track position of the center of the ellipse representing the final relative motion, and  $t^*$  is the bang-bang switching time. Note that the impulse delay  $\Delta t$  has to be lower than  $t^*/2$ . Moreover, the impulse magnitudes  $A_i$  are equal to 0.5 since the damping of the in-plane dynamics described by Eqs. (1) is zero.

### Zero Vibration Derivative Shaper

The formulation of the ZVD shaper is similar to that of the ZV shaper. However, the ZVD shaper provides higher robustness to modeling errors by forcing the derivative of the vibration amplitude with respect to the frequency to be zero.<sup>10</sup> The cost of the added robustness is a longer time to cancel the residual oscillation of the system. The ZVD consists of three impulses whose temporal distribution and magnitudes are

$$T = [t_1, t_2, t_3] = [0 \quad \Delta t \quad 2\Delta t] \quad (11)$$

$$A = [A_1, A_2, A_3] = \left[ \frac{\zeta^2}{\zeta^2 + 2\zeta + 1}, \frac{2\zeta}{\zeta^2 + 2\zeta + 1}, \frac{1}{\zeta^2 + 2\zeta + 1} \right] \quad (12)$$

with  $\zeta$  given by Eq. (8). In accordance with the analysis carried out in the previous section, the ZVD shaped input vector  $\mathbf{U} = [u\sin(\alpha), u\cos(\alpha)]^T$  can be formulated as follows:

$$\mathbf{u} = A_1 f_{t1} + A_2 f_{t2} + A_3 f_{t3} \quad (13)$$

where

$$f_{t1} = \begin{cases} 0 & t > t^* \\ \bar{u} \operatorname{sign}(\bar{y}_d - y_0) & t < t^*/2 \\ -\bar{u} \operatorname{sign}(\bar{y}_d - y_0) & t^*/2 < t < t^* \end{cases} \quad (14)$$

$$f_{t2} = f_{t1}(t - \Delta t)$$

$$f_{t3} = f_{t1}(t - 2\Delta t)$$

Here, the impulse delay  $\Delta t$  is constrained to be lower than  $t^*/4$  and the impulses' magnitudes are  $A_{1,3} = 1/4$  and  $A_2 = 1/2$ .

For the sake of example, Figure 1 shows the thrust profile shaped through the ZVD and ZV shapers respectively when  $\bar{y}_d < y_0$ .

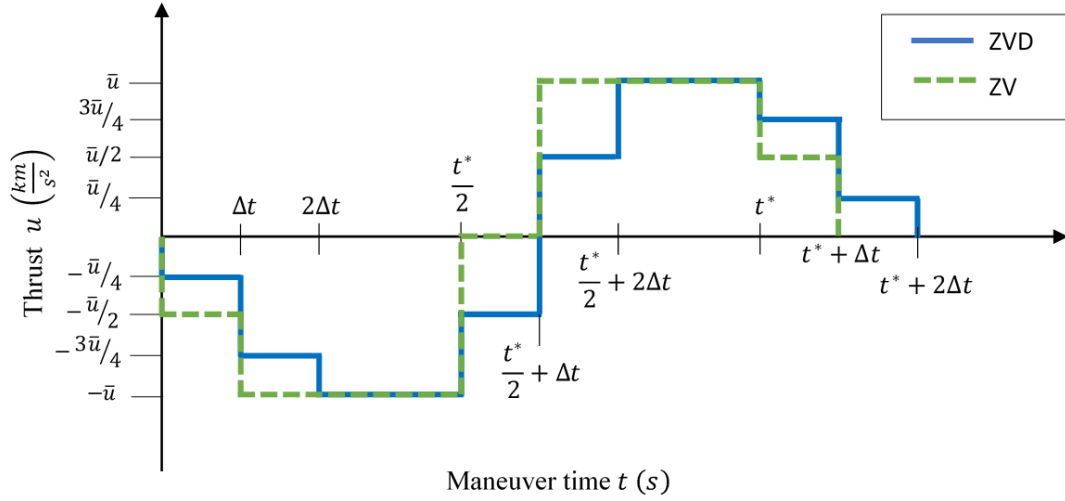


Figure 1. Shaped control profile

### INPUT SHAPING ANALYTICAL GUIDANCE

This section presents the steps to derive the closed-form solutions for final relative state and eccentricity when the ZV and ZVD shapers are implemented.

#### ZV Shaper

Using the analytical SS solution given by Eq. (4) with the filtered control signal given by Eqs. (9) and the generic initial condition  $\mathbf{X}_0 = [x_0 \ y_0 \ \dot{x}_0 \ \dot{y}_0]$ , the in-plane final state can be computed as given by Eq. (28) listed in Appendix A. The along-track location of the center of the ellipse representing the final relative orbit is given by the following formula<sup>11</sup>

$$\bar{y} = y_f - \frac{2\dot{x}_f \bar{m}}{\bar{n}^2}. \quad (15)$$

Using the expression of final state reported in Eq. (28), Eq. (15) can be rearranged as follows,

$$\begin{aligned} \bar{y} &= f(\mathbf{X}_0, t^*, \Delta t, \bar{m}, \bar{n}, \alpha, \bar{u}) \\ &= \frac{-1}{4\bar{n}^2} [8\bar{m}\dot{x}_0 - 4\bar{n}^2 y_0 + 32\bar{m}^3 t^* x_0 + 16\bar{m}^2 t^* \dot{y}_0 - 4\bar{n}^2 t^* \dot{y}_0 - 4\bar{m}^2 t^{*2} \bar{u}_y \\ &\quad + \bar{n}^2 t^{*2} \bar{u}_y + 32\Delta t \bar{m}^3 x_0 + 16\Delta t \bar{m}^2 \dot{y}_0 - 4\Delta t \bar{n}^2 \dot{y}_0 - 8\Delta t \bar{m} \bar{n}^2 x_0 \\ &\quad - 8\bar{m} \bar{n}^2 t^* x_0] \end{aligned} \quad (16)$$

where  $\bar{u}_y = \bar{u} \cos(\alpha)$  and  $\bar{u}_x = \bar{u} \sin(\alpha)$ . Then, Eq. (16) can be solved for the switching time  $t^*$  such that  $\bar{y}(t^*) = \bar{y}_d$ , i.e.

$$t^* = \frac{2}{\bar{u}_y (4\bar{m}^2 - \bar{n}^2)} [8\bar{m}^3 x_0 + 4\bar{m}^2 \dot{y}_0 - 2\bar{m} \bar{n}^2 x_0 - \bar{n}^2 \dot{y}_0 \pm A] \quad (17)$$

where

$$A = \sqrt{(4\bar{m}^2 - \bar{n}^2) \left( \begin{aligned} &16\bar{m}^4 x_0^2 + 4\bar{m}^2 \dot{y}_0^2 - \bar{n}^2 \dot{y}_0^2 - \bar{n}^2 \bar{u}_y y_0 + \bar{n}^2 \bar{u}_y \bar{y}_d \\ &+ 16\bar{m}^3 x_0 \dot{y}_0 + 2\bar{m} \bar{u}_y \dot{x}_0 - 4\bar{m}^2 \bar{n}^2 x_0^2 + 8\Delta t \bar{m}^3 \bar{u}_y x_0 \\ &+ 4\Delta t \bar{m}^2 \bar{u}_y \dot{y}_0 - \Delta t \bar{n}^2 \bar{u}_y \dot{y}_0 - 4\bar{m} \bar{n}^2 x_0 \dot{y}_0 - 2\Delta t \bar{m} \bar{n}^2 \bar{u}_y x_0 \end{aligned} \right)} \quad (18)$$

In order to obtain a closed, non-drifting relative orbit at the end of maneuver, the following conditions must be satisfied<sup>12</sup>:

$$\dot{y}_f = -2\bar{m}x_f \quad (19)$$

or

$$\bar{x} = 4x_f + \frac{2\dot{y}_f}{\bar{m}} = 0 \quad (20)$$

where  $\bar{x}$  represents the radial location of the center of the final ellipse. Using the final state equations obtained through the application of the shaped control profile, i.e. Eq. (28), the term  $\bar{x}$  becomes

$$\bar{x} = 4x_f + \frac{2\dot{y}_f}{\bar{m}} = 4x_0 + \frac{2\dot{y}_0}{\bar{m}}. \quad (21)$$

This indicates that the application of thrust profile described by Eqs. (9)-(10) guarantees a non-drifting closed relative orbit if the initial motion is an equilibrium. The eccentricity of the final relative orbit is given by the following formula (Reference 11)

$$e_{rel} = \sqrt{(x_f - \bar{x})^2 + ((y_f - \bar{y})/2)^2}. \quad (22)$$

The relative eccentricity can be written as a function of  $\mathbf{X}_0, t^*, \Delta t, \bar{m}, \bar{n}, \bar{u}$  and  $\alpha$ , substituting the expression of final state (Appendix A, Eq. (28)) in Eq. (22). The final form is listed as Eq. (30) (see Appendix C).

### ZVD Shaper

Substituting the ZVD control signal given by Eq. (13) in Eq. (4), considering a set of generic initial condition  $\mathbf{X}_0 = [x_0 \ y_0 \ \dot{x}_0 \ \dot{y}_0]$ , leads to the final state reported in Eq. (29) (see Appendix B). As discussed in the previous section for ZV shaper, the along-track location of the center of the final relative ellipse is given by the following formula,

$$\bar{y} = y_f - \frac{2\dot{x}_f\bar{m}}{\bar{n}^2} = \frac{-1}{4\bar{n}^2} [8\bar{m}\dot{x}_0 - 4\bar{n}^2y_0 + 32\bar{m}^3t^*x_0 + 16\bar{m}^2t^*\dot{y}_0 - 4\bar{n}^2t^*\dot{y}_0 - 4\bar{m}^2t^{*2}\bar{u}_y + \bar{n}^2t^{*2}\bar{u}_y + 64\Delta t\bar{m}^3x_0 + 32\Delta t\bar{m}^2\dot{y}_0 - 8\Delta t\bar{n}^2\dot{y}_0 - 16\Delta t\bar{m}\bar{n}^2x_0 - 8\bar{m}\bar{n}^2t^*x_0]. \quad (23)$$

The switching time  $t^*$  can be computed by solving  $\bar{y}(t^*) = \bar{y}_d$ , which yields

$$t^* = \frac{2}{\bar{u}_y(4\bar{m}^2 - \bar{n}^2)} [8\bar{m}^3x_0 + 4\bar{m}^2\dot{y}_0 - 2\bar{m}\bar{n}^2x_0 - \bar{n}^2\dot{y}_0 \pm A] \quad (24)$$

where

$$A = \sqrt{(4\bar{m}^2 - \bar{n}^2) \left( \begin{array}{l} 16\bar{m}^4x_0^2 + 4\bar{m}^2\dot{y}_0^2 - \bar{n}^2\dot{y}_0^2 - \bar{n}^2\bar{u}_y y_0 + \bar{n}^2\bar{u}_y \bar{y}_d \\ + 16\bar{m}^3x_0\dot{y}_0 + 2\bar{m}\bar{u}_y\dot{x}_0 - 4\bar{m}^2\bar{n}^2x_0^2 + 16\Delta t\bar{m}^3\bar{u}_y x_0 \\ + 8\Delta t\bar{m}^2\bar{u}_y\dot{y}_0 - 2\Delta t\bar{n}^2\bar{u}_y\dot{y}_0 - 4\bar{m}\bar{n}^2x_0\dot{y}_0 - 4\Delta t\bar{m}\bar{n}^2\bar{u}_y x_0 \end{array} \right)} \quad (25)$$

Also for the ZVD case, the non-drifting condition  $\bar{x} = 0$  (i.e.,  $\dot{y}_f = -2\bar{m}x_f$ ) at the end of the maneuver  $t_m = t^* + 2\Delta t$  is satisfied if the initial motion is an equilibrium. In other words, the Eq. (21) is still valid.

Ultimately, the eccentricity of the final relative orbit can be computed through the Eq. (22) and Eq. (29), and is listed in Appendix D as Eq. (31).

### NUMERICAL SIMULATIONS

This section presents the guidance trajectories obtained using the thrust profile derived in the previous sections and the orbital parameters listed in Table 1. It is worth noting that for the following simulations, the initial orbital parameters summarized in Table 1 are first converted to Cartesian position and velocity in an Earth-centered inertial frame, then translated kinematically into the LVLH frame.

**Table 1: Initial orbital parameters for spacecraft**

Orbital Parameter	Chief	Deputy
Semi-major axis $a$	6778.1 km	6778.1 km
Eccentricity $e$	0	0.0001
Inclination $i$	97.9908 deg	97.9908 deg
Right ascension of ascending node (RAAN) $\Omega$	261.621 deg	261.621 deg
Argument of perigee $\omega$	30 deg	30 deg
Polar angle $\nu$	27.216 deg	27.18 deg

Two different scenarios are considered hereafter. For the first one (Case 1), initial relative state deriving from the initial orbital parameters is forced to match a leader-follower initial condition for the linear equations (1), i.e. cancelling  $x$  displacement and both relative velocity components. For the second scenario (Case 2) they are forced to match the equilibrium motion initial condition, i.e.  $y_0 = -2\bar{m}x_0$ . Table 2 summarizes the initial relative state,  $\mathbf{X}_0$ , for both scenarios.

**Table 2: Initial state  $\mathbf{X}_0$  for studied cases**

Simulation Scenarios	$x$ (km)	$y_0$ (km)	$\dot{x}_0$ (km/s)	$\dot{y}_0$ (km/s)
<b>CASE 1</b>	0	-4.258	0	0
<b>CASE 2</b>	-0.604	-4.258	0.0004	0.0014

The initial relative eccentricity,

$$e_{rel,0} = \sqrt{\left[ x_0 - \left( 4x_0 + \frac{2y_0}{\bar{m}} \right) \right]^2 + \left[ \frac{y_0 - \left( y_0 + \frac{2x_0\bar{m}}{n^2} \right)}{2} \right]^2}, \quad (26)$$

for Cases 1 and 2 is 0 and 0.6792 respectively. For all sample cases, the maximum thrust magnitude is assumed  $\bar{u} = 2 \cdot 10^{-8} km/s^2$ .

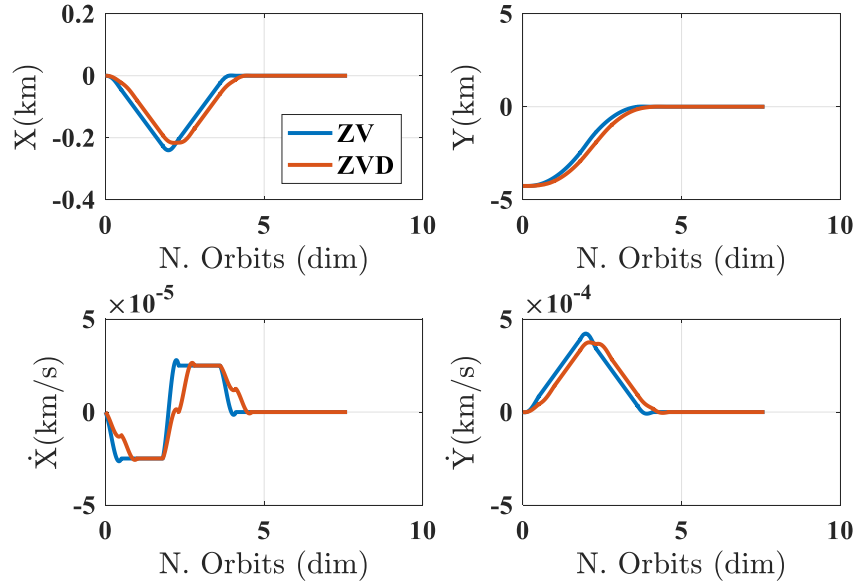
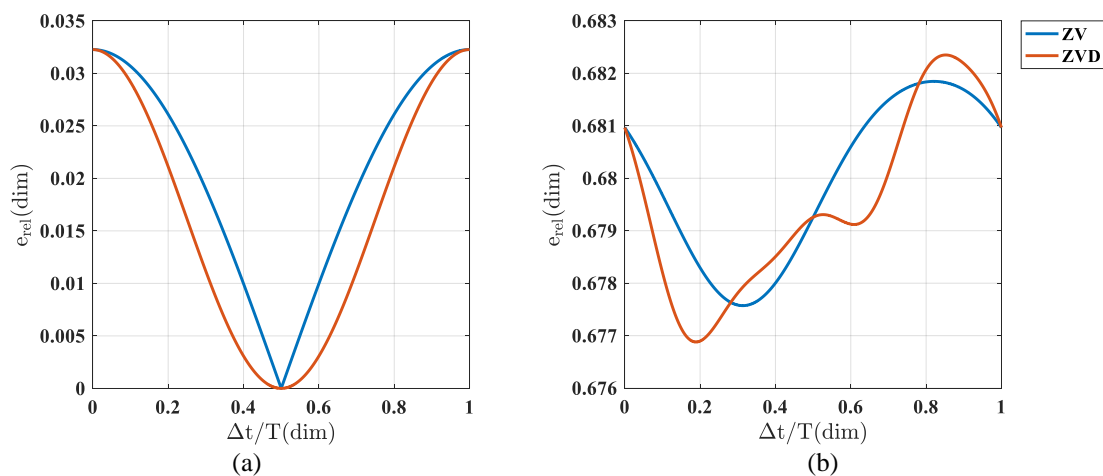


**Figure 2: Relative state vector components**

As a first example, for Case 1 with  $\alpha = 45^\circ$  and  $\Delta t/T = 0.5$ , with  $T = 2\pi/\bar{n}$ , the relative state components evolve over the course of the maneuver time,  $t_m = t^* + \Delta t$  and  $t_m = t^* + 2\Delta t$  for ZV and ZVD respectively, according to Figure 2. It can be verified by this example that using the ZVD shaper results in a longer time than ZV shaper to nullify the oscillations introduced to the system by the control accelerations.

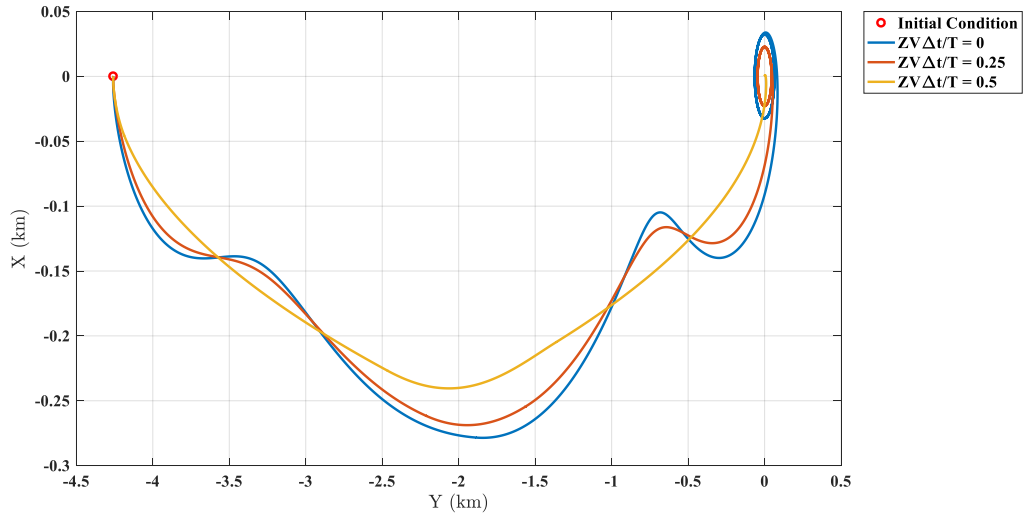
In Figure 3 the equations of final relative eccentricity, Eqs. (30)-(31), are plotted over a range of  $\Delta t/T$  values, for Case 1 (left) and Case 2 (right) when  $\alpha = 45^\circ$ . For Case 1 the minimum final relative eccentricity,  $e_{rel}$ , is zero when  $\Delta t/T = 0.5$  for both ZV and ZVD shapers. The maximum  $e_{rel}$  is obtained when  $\Delta t/T = 0$  or  $\Delta t/T = 1$  for both classes of shapers. Note that the value of  $\Delta t$  has to be lower than  $t^*/2$  and  $t^*/4$  for ZV and ZVD solutions respectively. In light of this, since the switching time,  $t^*$ , is 5.57 hrs and 5.962 hrs for Case 1 and Case 2 respectively, the value of  $\Delta t/T$  has to be 0.9 at most when the ZVD shaper is implemented, for both simulated cases.

For Case 2 using the ZV shaper,  $\Delta t/T = 0.3134$  yields the minimum  $e_{rel}$  and  $\Delta t/T = 0.8209$  yields the maximum  $e_{rel}$ . Additionally when the ZVD shaper is used,  $\Delta t/T = 0.1891$  yields the minimum  $e_{rel}$  and  $\Delta t/T = 0.8519$  yields the maximum  $e_{rel}$ . For Case 2, it is clear that neither shaper can completely damp the system oscillation (i.e., force  $e_{rel}$  to zero). In fact, the shapers are designed to suppress the vibrations introduced by maneuver control input, rather than to cancel the existing initial oscillations. However, for both cases and both shapers, the final relative eccentricity matches the initial relative eccentricity when  $\Delta t/T = 0.5$ .

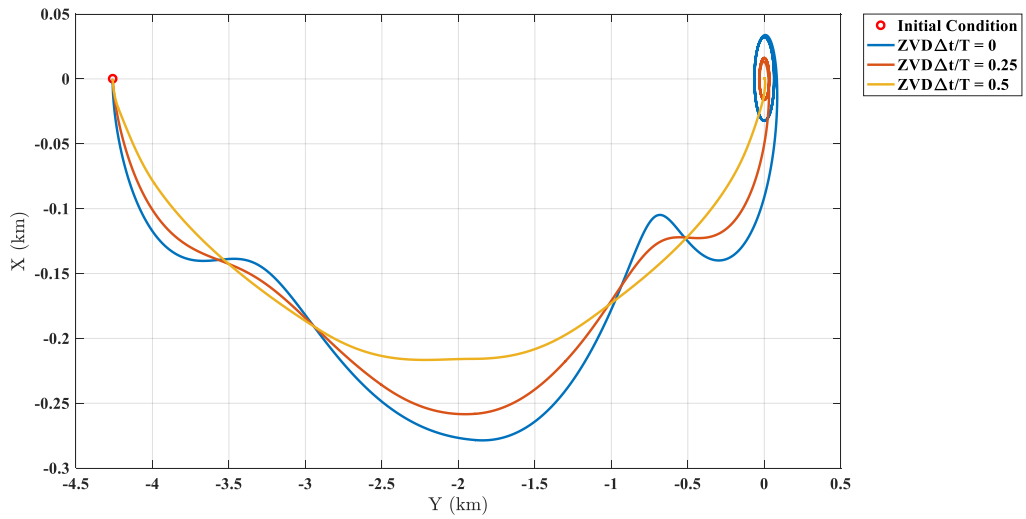


**Figure 3:  $e_{rel}$  vs.  $\Delta t/T$  for Case 1 (a) and Case 2 (b)**

In the following figures, guidance trajectories are plotted for each case and each shaper using the values of  $\Delta t/T$  calculated above when  $\alpha = 45^\circ$ . The three plots in each figure use  $\Delta t/T$  values which result in minimum, intermediate, and maximum final relative eccentricity.



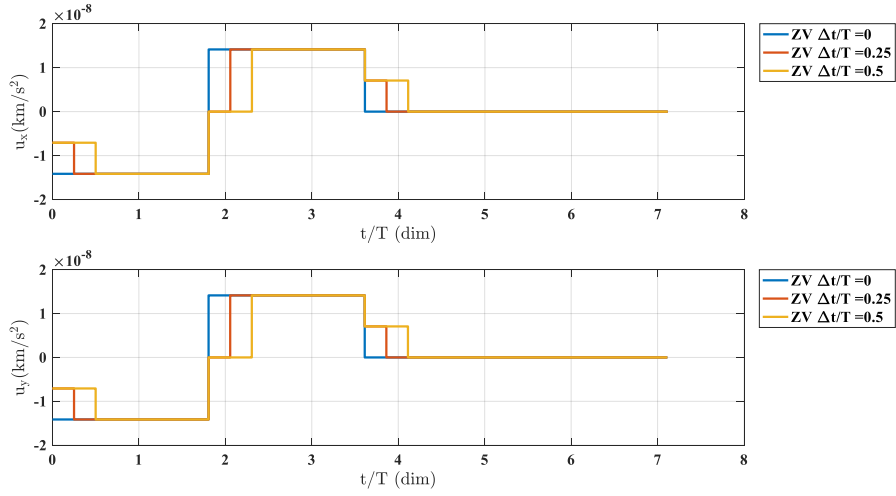
**Figure 4: Guidance trajectories given by ZV shaper for Case 1**



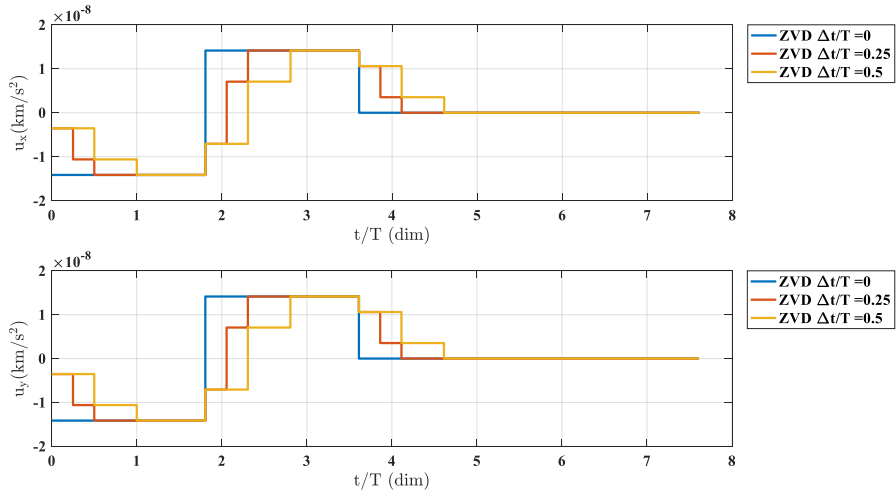
**Figure 5: Guidance trajectories given by ZVD shaper for Case 1**

Figure 4 and Figure 5 show trajectories using Case 1 initial conditions when the ZV and ZVD are applied respectively. The values of  $\Delta t/T$  used are 0 (for max  $e_{rel}$ ), 0.25 (for intermediate  $e_{rel}$ ), and 0.5 (for min  $e_{rel}$ ).

Figure 6 and Figure 7 show the control input components corresponding to the trajectories shown in Figure 4 and Figure 5, when the ZV and ZVD shapers are applied respectively.



**Figure 6: Control profile shaped by ZV for Case 1**



**Figure 7: Control profile shaped by ZVD for Case 1**

Figure 8 and Figure 9 illustrate the guidance trajectories using Case 2 initial conditions when the ZV and ZVD shapers are applied respectively. The values of  $\Delta t/T$  used are 0.8209 (for max  $e_{rel}$ ), 0.5 (for  $e_{rel} = e_{rel,0}$ ), and 0.3134 (for min  $e_{rel}$ ) when the ZV shaper is applied and 0.8519 (for max  $e_{rel}$ ), 0.5 (for  $e_{rel} = e_{rel,0}$ ), and 0.1891 (for min  $e_{rel}$ ) when the ZVD shaper is applied.

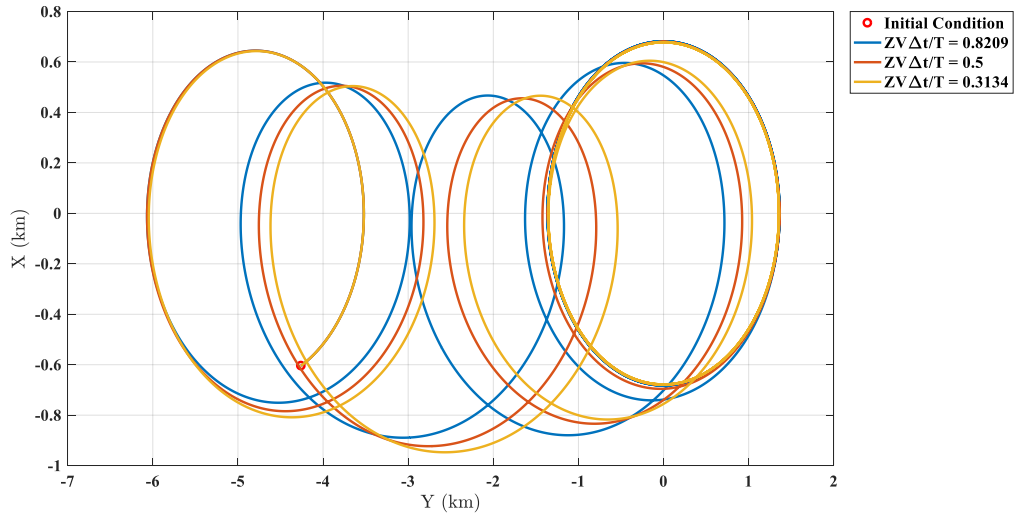


**Figure 8: Guidance trajectories given by ZV shaper for Case 2**

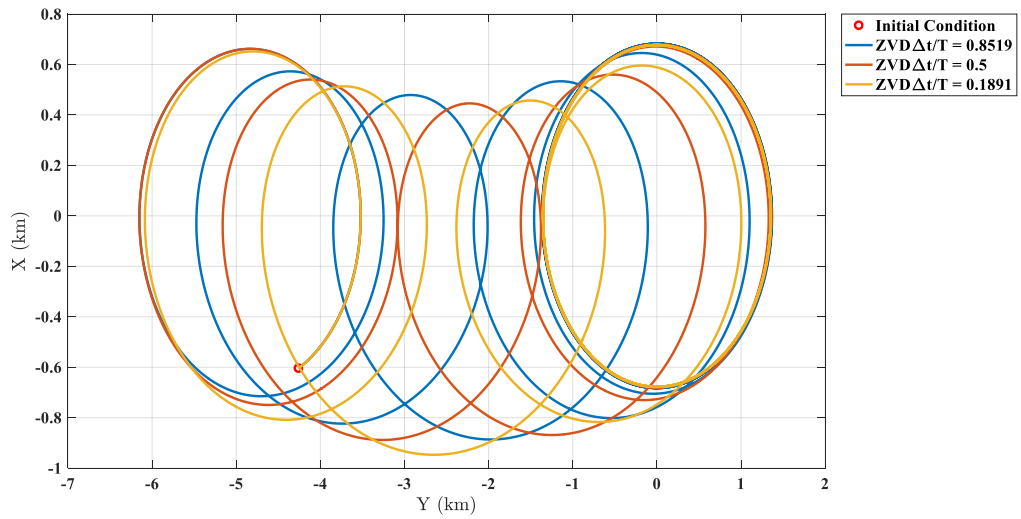


**Figure 9: Guidance trajectories given by ZVD shaper for Case 2**

Figure 10 and Figure 11 show the control input components corresponding to the trajectories shown in Figure 8 and Figure 9 for both ZV and ZVD.

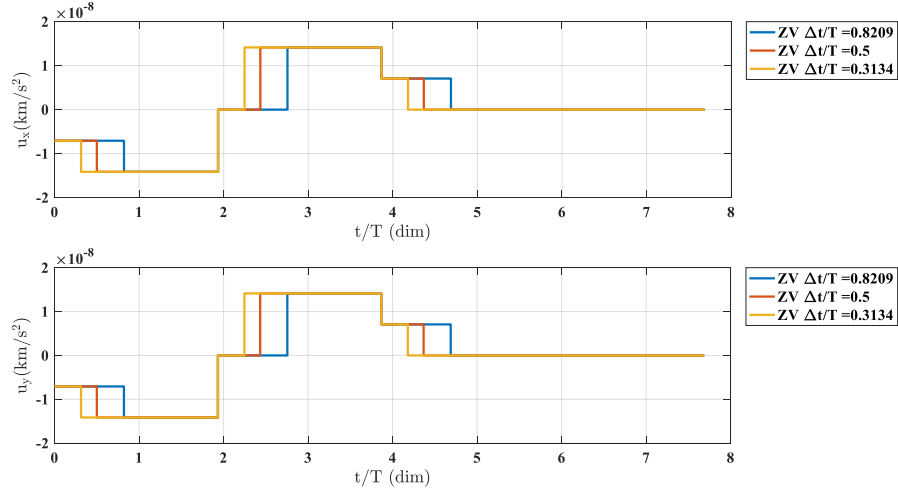


Figure 10: Control profile shaped by ZV for Case 2

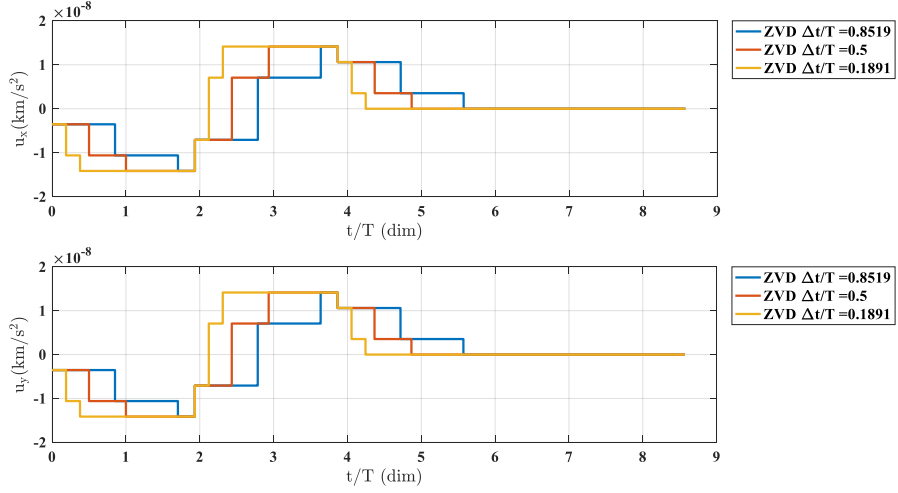


Figure 11: Control profile shaped by ZVD for Case 2

## OPTIMAL GUIDANCE SOLUTION

As discussed in the previous sections, the control vector,  $\mathbf{U}$ , depends on shaper delay  $\Delta t$  and thrust angle  $\alpha$ , once the parameters  $\bar{\mathbf{u}}$  and  $y_{fd}$  are set and the initial state  $\mathbf{X}_0$  is given. In this study, a gradient-based algorithm is proposed to find the values of  $\Delta t$  and  $\alpha$  that minimize the maneuver cost in terms of  $\Delta V = \bar{\mathbf{u}}(t^*(\alpha) - \Delta t)$ , satisfying the following constraints

$$\begin{aligned}
 & |e_{rel}(\Delta t, \alpha) - e_{rel,d}| = 0 \\
 & \begin{cases} \frac{t^*(\alpha)}{2} - 2\Delta T > 0 & \text{for ZVD} \\ \frac{t^*(\alpha)}{2} - \Delta T > 0 & \text{for ZV} \end{cases} \quad (27)
 \end{aligned}$$

where  $e_{rel,d}$  is the desired final relative eccentricity. MATLAB's *fmincon SQP* routine is used to solve the above optimization problem. For the sake of simplicity only the optimal solution associated with the ZVD shaper is presented hereafter. However, the same approach might be extended to the ZV related solution.

In order to get insight into the permissible values of final relative eccentricity and facilitate the definition of space search bounds for the optimizer, a parametric analysis was carried out showing the relationships between  $\Delta V$  and  $e_{rel}$  and the optimizer variables,  $\alpha$ ,  $\Delta t$ , given a set of initial conditions  $X_0$  and the design parameters  $\bar{u}$  and  $y_{fd}$ . Thus, Figure 12 shows the surface of  $\Delta V$  vs.  $\alpha$  vs.  $\Delta t/T$ , taking into account the constraints on  $\Delta t$ , i.e.  $\Delta t < t^*/4$ . For the presented analysis the Case 2 initial conditions are used. From the figure it is straightforward that the total maneuver  $\Delta V$  decreases when the thrust angle converges to zero value and the ratio  $\Delta t/T$  increases up to 0.812. Figure 13 illustrates the surface of  $e_{rel}$  vs.  $\alpha$  vs.  $\Delta t/T$ . Again the constraint  $\Delta t < t^*/4$  is taken into account and the Case 2 initial conditions are used. From the figure it is clear that the achievable values of the final relative eccentricity by using the input-shaping based solution lie in the range [0.6128, 0.7838]. In addition, it is worth remarking that the parametric analysis can be exploited to determine a “good” initial guess, improving the convergence performance of the optimizer, and assess the optimizer solution.

Assuming a desired value for the final eccentricity of 0.7, the optimizer gives the solution  $\Delta t/T = 0.24416$  and  $\alpha = 1.3692 \text{ deg}$  with  $\Delta V = 0.334 \text{ m/s}$ . This point is shown among the initial guess ( $\Delta t/T = 0.5$ ,  $\alpha = 0^\circ$ ), which leads to  $\Delta V = 0.305 \text{ m/s}$ , in the plots reported in Figure 12 and Figure 13 below.

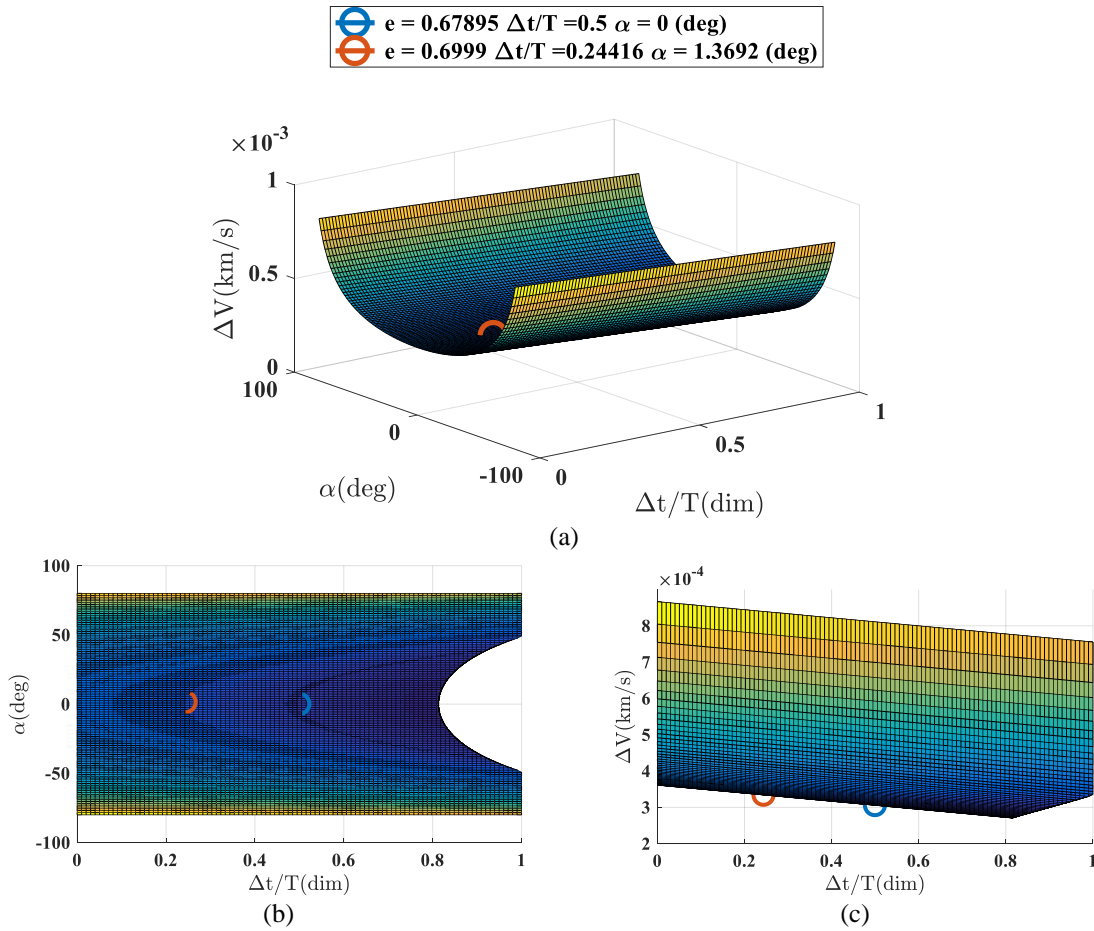
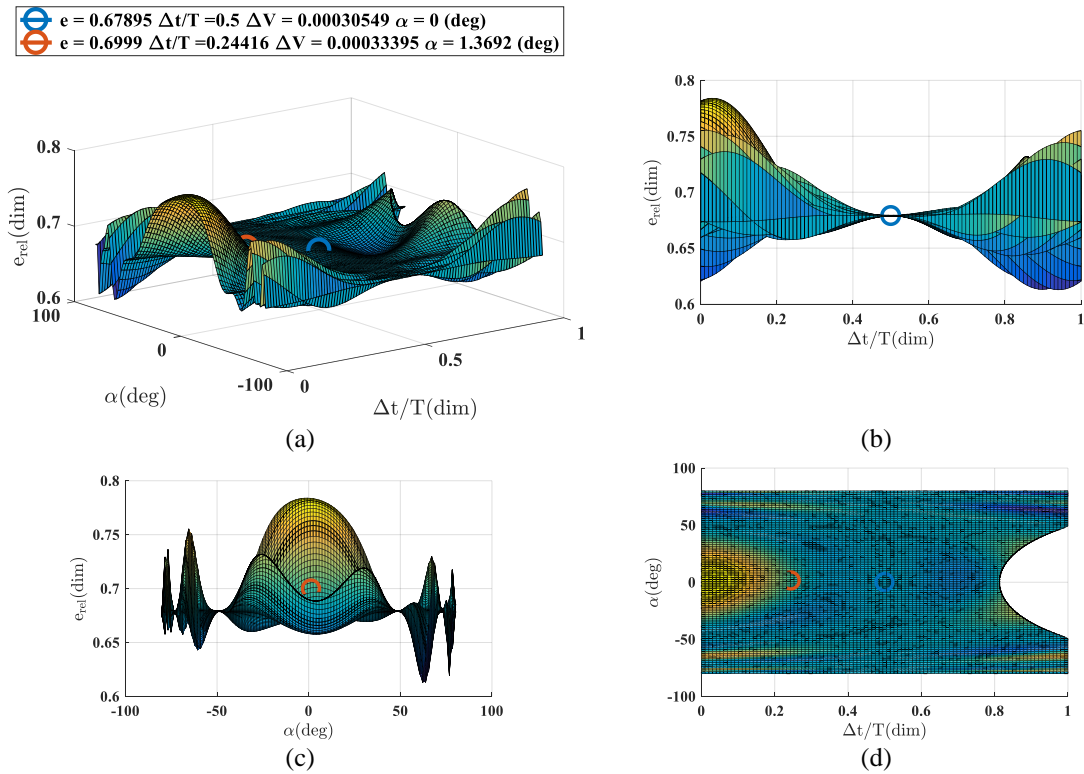
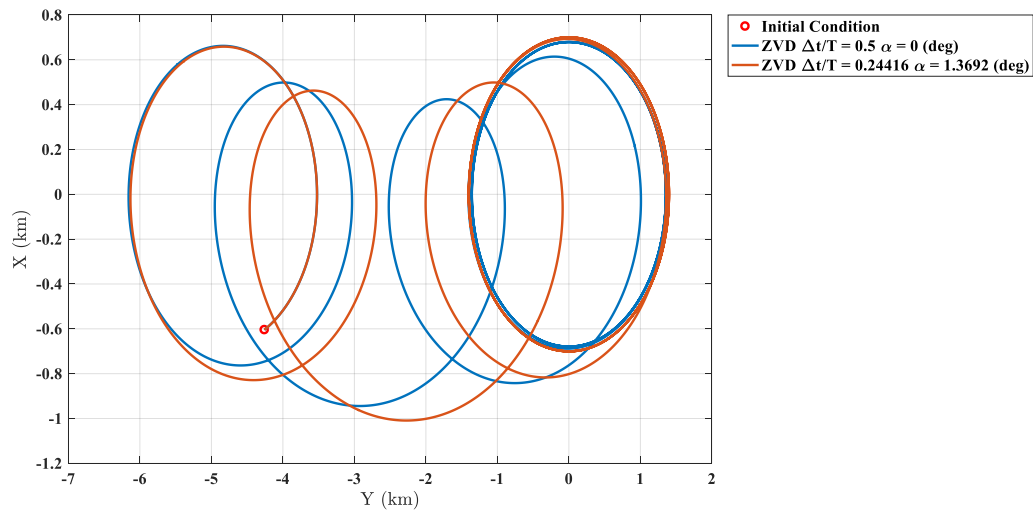


Figure 12.  $\Delta V$  vs.  $\alpha$  vs.  $\Delta t/T$  (a). Projection of  $\Delta V$  on  $\alpha - \Delta t/T$  plane (b), and on  $\Delta V - \Delta t/T$  plane (c)



**Figure 13.  $e_{rel}$  vs.  $\alpha$  vs.  $\Delta t/T$  (a). Projection of  $e_{rel}$  on.  $e_{rel} - \Delta t/T$  plane (b), on  $e_{rel} - \alpha$  plane (c), and.  $\alpha - \Delta t/T$  plane (d)**

Figure 14 shows the trajectory corresponding with the initial guess ( $\Delta t/T = 0.5$ ,  $\alpha = 0^\circ$ ) and optimal solution ( $\Delta t/T = 0.24416$ ,  $\alpha = 1.3692^\circ$ ). Figure 15 shows the  $x$  and  $y$  control profiles of each set of conditions over the maneuver time.



**Figure 14. Guidance trajectory**

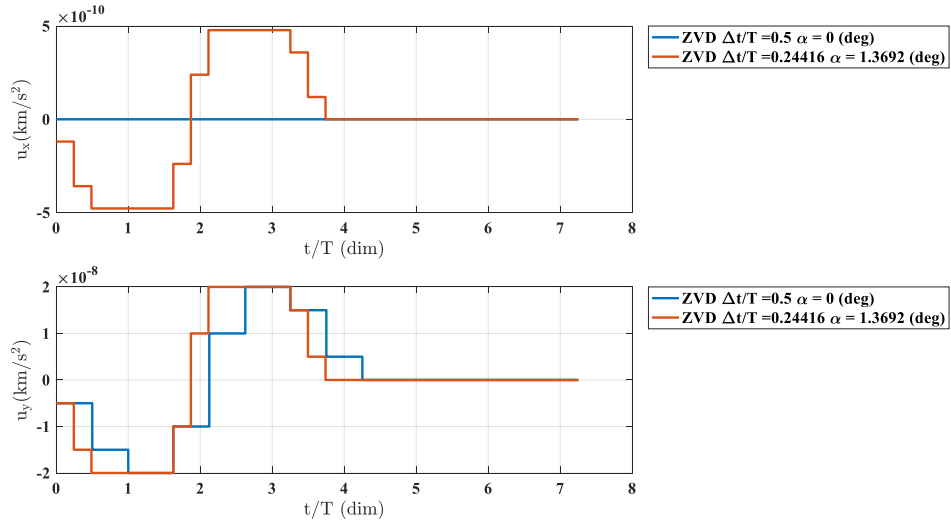


**Figure 15. Control profile**

## CONCLUSION

The results presented in this paper demonstrate that input shaping theory can be exploited to derive a general analytical guidance solution for relative orbital maneuvering as a function of shaper delay,  $\Delta t$ , and thrust angle,  $\alpha$ . The computed solutions allow a spacecraft to move from an initial location along its orbit to a desired position on the same course as well as to fly around a desired point placed ahead or behind its initial position. It is worth remarking that the derived trajectories bring the spacecraft from an equilibrium configuration to a new equilibrium one, where equilibrium means a non-drifting relative state.

The main contribution of this paper consists of deriving an analytical guidance solution, including the effects of  $J_2$  perturbation, for planar spacecraft rephasing and rendezvous maneuvers. This could be easily implemented onboard small spacecraft with a low-thrust propulsion system and limited computing capabilities. The second important contribution is the ability to use such analytical solutions to easily and quickly compute maneuvers that require minimum fuel consumption.

## ACKNOWLEDGEMENTS

The authors thank the US Air Force Research Laboratory and Stanford University for sponsoring this investigation under contract # FA9453-16-C-0029.

## APPENDIX A: ZV FINAL STATE

$$\begin{aligned}
x_f &= \frac{1}{2\bar{n}^3} \left[ \bar{n}\bar{u}_x + 8\bar{m}^2\bar{n}x_0 + \bar{n}\bar{u}_x \cos(\bar{n}(\Delta t + t^*)) + 2\bar{m}\bar{u}_y \sin(\bar{n}(\Delta t + t^*)) + 4\bar{m}\bar{n}\dot{y}_0 \right. \\
&\quad + \bar{n}\bar{u}_x \cos(\bar{n}\Delta t) + 2\bar{m}\bar{u}_y \sin(\bar{n}\Delta t) + \bar{n}\bar{u}_x \cos(\bar{n}t^*) - 2\bar{n}\bar{u}_x \cos(\bar{n}t^*/2) \\
&\quad - 2\bar{n}\bar{u}_x \cos(\bar{n}(2\Delta t + t^*)/2) + 2\bar{n}^3x_0 \cos(\bar{n}(\Delta t + t^*)) + 2\bar{m}\bar{u}_y \sin(\bar{n}t^*) \\
&\quad - 4\bar{m}\bar{u}_y \sin(\bar{n}t^*/2) - 4\bar{m}\bar{u}_y \sin(\bar{n}(2\Delta t + t^*)/2) \\
&\quad + 2\bar{n}^2\dot{x}_0 \sin(\bar{n}(\Delta t + t^*)) - 8\bar{m}^2\bar{n}x_0 \cos(\bar{n}(\Delta t + t^*)) \\
&\quad \left. - 4\bar{m}\bar{n}\dot{y}_0 \cos(\bar{n}(\Delta t + t^*)) \right] \\
y_f &= \frac{1}{4\bar{n}^4} \left[ 8\bar{m}^2\bar{u}_y + 4\bar{n}^4y_0 - 8\bar{m}\bar{n}^2\dot{x}_0 + 8\bar{m}^2\bar{u}_y \cos(\bar{n}\Delta t) + 4\bar{n}^4t^*\dot{y}_0 + 8\bar{m}^2\bar{u}_y \cos(\bar{n}t^*) \right. \\
&\quad - 16\bar{m}^2\bar{u}_y \cos(\bar{n}t^*/2) - 16\bar{m}^2\bar{u}_y \cos(\bar{n}(2\Delta t + t^*)/2) - \bar{n}^4t^{*2}\bar{u}_y \\
&\quad + 4\Delta t\bar{n}^4\dot{y}_0 + 8\bar{m}^2\bar{u}_y \cos(\bar{n}(\Delta t + t^*)) - 4\bar{m}\bar{n}\bar{u}_x \sin(\bar{n}(\Delta t + t^*)) \\
&\quad - 4\bar{m}\bar{n}\bar{u}_x \sin(\bar{n}\Delta t) + 4\bar{m}^2\bar{n}^2t^{*2}\bar{u}_y + 8\Delta t\bar{m}\bar{n}^4x_0 \\
&\quad + 8\bar{m}\bar{n}^2\dot{x}_0 \cos(\bar{n}(\Delta t + t^*)) - 4\bar{m}\bar{n}\bar{u}_x \sin(\bar{n}t^*) + 8\bar{m}\bar{n}\bar{u}_x \sin(\bar{n}t^*/2) \\
&\quad + 8\bar{m}\bar{n}\bar{u}_x \sin(\bar{n}(2\Delta t + t^*)/2) - 8\bar{m}\bar{n}^3x_0 \sin(\bar{n}(\Delta t + t^*)) \\
&\quad + 32\bar{m}^3\bar{n}x_0 \sin(\bar{n}(\Delta t + t^*)) + 16\bar{m}^2\bar{n}\dot{y}_0 \sin(\bar{n}(\Delta t + t^*)) + 8\bar{m}\bar{n}^4t^*x_0 \\
&\quad \left. - 32\Delta t\bar{m}^3\bar{n}^2x_0 - 16\Delta t\bar{m}^2\bar{n}^2\dot{y}_0 - 32\bar{m}^3\bar{n}^2t^*x_0 - 16\bar{m}^2\bar{n}^2t^*\dot{y}_0 \right] \tag{28} \\
\dot{x}_f &= \frac{1}{\bar{n}^2} \left[ \bar{m}\bar{u}_y + \bar{m}\bar{u}_y \cos(\bar{n}(\Delta t + t^*)) - \bar{n}\bar{u}_x \sin(\bar{n}(\Delta t + t^*)) / 2 + \bar{m}\bar{u}_y \cos(\bar{n}\Delta t) \right. \\
&\quad - \bar{n}\bar{u}_x \sin(\bar{n}\Delta t) / 2 + \bar{m}\bar{u}_y \cos(\bar{n}t^*) - 2\bar{m}\bar{u}_y \cos(\bar{n}t^*/2) \\
&\quad - 2\bar{m}\bar{u}_y \cos(\bar{n}(2\Delta t + t^*)/2) + \bar{n}^2\dot{x}_0 \cos(\bar{n}(\Delta t + t^*)) - \bar{n}\bar{u}_x \sin(\bar{n}t^*) / 2 \\
&\quad + \bar{n}\bar{u}_x \sin(\bar{n}t^*/2) + \bar{n}\bar{u}_x \sin(\bar{n}(2\Delta t + t^*)/2) - \bar{n}^3x_0 \sin(\bar{n}(\Delta t + t^*)) \\
&\quad \left. + 2\bar{m}\bar{n}\dot{y}_0 \sin(\bar{n}(\Delta t + t^*)) + 4\bar{m}^2\bar{n}x_0 \sin(\bar{n}(\Delta t + t^*)) \right] \\
\dot{y}_f &= -\frac{1}{\bar{n}^3} \left[ 8\bar{m}^3\bar{n}x_0 - 2\bar{m}\bar{n}^3x_0 - \bar{n}^3\dot{y}_0 + 4\bar{m}^2\bar{n}\dot{y}_0 + 2\bar{m}^2\bar{u}_y \sin(\bar{n}\Delta t) + 2\bar{m}^2\bar{u}_y \sin(\bar{n}t^*) \right. \\
&\quad - 4\bar{m}^2\bar{u}_y \sin(\bar{n}t^*/2) - 4\bar{m}^2\bar{u}_y \sin(\bar{n}(2\Delta t + t^*)/2) + \bar{m}\bar{n}\bar{u}_x \\
&\quad + 2\bar{m}^2\bar{u}_y \sin(\bar{n}(\Delta t + t^*)) + \bar{m}\bar{n}\bar{u}_x \cos(\bar{n}\Delta t) + \bar{m}\bar{n}\bar{u}_x \cos(\bar{n}t^*) \\
&\quad - 2\bar{m}\bar{n}\bar{u}_x \cos(\bar{n}t^*/2) - 2\bar{m}\bar{n}\bar{u}_x \cos(\bar{n}(2\Delta t + t^*)/2) \\
&\quad + 2\bar{m}\bar{n}^3x_0 \cos(\bar{n}(\Delta t + t^*)) - 8\bar{m}^3\bar{n}x_0 \cos(\bar{n}(\Delta t + t^*)) \\
&\quad - 4\bar{m}^2\bar{n}\dot{y}_0 \cos(\bar{n}(\Delta t + t^*)) + 2\bar{m}\bar{n}^2\dot{x}_0 \sin(\bar{n}(\Delta t + t^*)) \\
&\quad \left. + \bar{m}\bar{n}\bar{u}_x \cos(\bar{n}(\Delta t + t^*)) \right] \\
\bar{u}_x &= \bar{u} \sin \alpha \\
\bar{u}_y &= \bar{u} \cos \alpha
\end{aligned}$$

## APPENDIX B: ZVD FINAL STATE

$$\begin{aligned}
x_f &= \frac{1}{4\bar{n}^3} \left[ \bar{n}\bar{u}_x + 16\bar{m}^2\bar{n}x_0 + 4\bar{n}^3x_0 \cos(\bar{n}(2\Delta t + t^*)) + 4\bar{n}^2\dot{x}_0 \sin(\bar{n}(2\Delta t + t^*)) \right. \\
&\quad + 2\bar{n}\bar{u}_x \cos(\bar{n}(\Delta t + t^*)) + 4\bar{m}\bar{u}_y \sin(\bar{n}(\Delta t + t^*)) + 8\bar{m}\bar{n}\dot{y}_0 \\
&\quad + 2\bar{n}\bar{u}_x \cos(\bar{n}\Delta t) + \bar{n}\bar{u}_x \cos(2\bar{n}\Delta t) + 4\bar{m}\bar{u}_y \sin(\bar{n}\Delta t) + 2\bar{m}\bar{u}_y \sin(2\bar{n}\Delta t) \\
&\quad + \bar{n}\bar{u}_x \cos(\bar{n}t^*) - 2\bar{n}\bar{u}_x \cos(\bar{n}t^*/2) + \bar{n}\bar{u}_x \cos(\bar{n}(2\Delta t + t^*)) \\
&\quad - 4\bar{n}\bar{u}_x \cos(\bar{n}(2\Delta t + t^*)/2) - 2\bar{n}\bar{u}_x \cos(\bar{n}(4\Delta t + t^*)/2) + 2\bar{m}\bar{u}_y \sin(\bar{n}t^*) \\
&\quad - 4\bar{m}\bar{u}_y \sin(\bar{n}t^*/2) + 2\bar{m}\bar{u}_y \sin(\bar{n}(2\Delta t + t^*)) \\
&\quad - 8\bar{m}\bar{u}_y \sin(\bar{n}(2\Delta t + t^*)/2) - 4\bar{m}\bar{u}_y \sin(\bar{n}(4\Delta t + t^*)/2) \\
&\quad \left. - 8\bar{m}\bar{n}\dot{y}_0 \cos(\bar{n}(2\Delta t + t^*)) - 16\bar{m}^2\bar{n}x_0 \cos(\bar{n}(2\Delta t + t^*)) \right] \\
y_f &= \frac{1}{4\bar{n}^4} \left[ 4\bar{m}^2\bar{u}_y + 4\bar{n}^4y_0 - 8\bar{m}\bar{n}^2\dot{x}_0 + 8\bar{m}^2\bar{u}_y \cos(\bar{n}\Delta t) + 4\bar{m}^2\bar{u}_y \cos(2\bar{n}\Delta t) + 4\bar{n}^4t^*\dot{y}_0 \right. \\
&\quad + 4\bar{m}^2\bar{u}_y \cos(\bar{n}\Delta t) - 8\bar{m}^2\bar{u}_y \cos(\bar{n}t^*/2) + 4\bar{m}^2\bar{u}_y \cos(\bar{n}(2\Delta t + t^*)) \\
&\quad - 16\bar{m}^2\bar{u}_y \cos(\bar{n}(2\Delta t + t^*)/2) - 8\bar{m}^2\bar{u}_y \cos(\bar{n}(4\Delta t + t^*)/2) - \bar{n}^4t^{*2}\bar{u}_y \\
&\quad + 8\Delta t\bar{n}^4\dot{y}_0 + 8\bar{m}^2\bar{u}_y \cos(\bar{n}(\Delta t + t^*)) - 4\bar{m}\bar{n}\bar{u}_x \sin(\bar{n}(\Delta t + t^*)) \\
&\quad - 4\bar{m}\bar{n}\bar{u}_x \sin(\bar{n}\Delta t) - 2\bar{m}\bar{n}\bar{u}_x \sin(2\bar{n}\Delta t) + 4\bar{m}^2\bar{n}^2t^{*2}\bar{u}_y + 16\Delta t\bar{m}\bar{n}^4x_0 \\
&\quad - 2\bar{m}\bar{n}\bar{u}_x \sin(\bar{n}t^*) + 4\bar{m}\bar{n}\bar{u}_x \sin(\bar{n}t^*/2) - 2\bar{m}\bar{n}\bar{u}_x \sin(\bar{n}(2\Delta t + t^*)) \\
&\quad + 8\bar{m}\bar{n}\bar{u}_x \sin(\bar{n}(2\Delta t + t^*)/2) + 4\bar{m}\bar{n}\bar{u}_x \sin(\bar{n}(4\Delta t + t^*)/2) + 8\bar{m}\bar{n}^4t^*x_0 \\
&\quad - 64\Delta t\bar{m}^3\bar{n}^2x_0 - 32\Delta t\bar{m}^2\bar{n}^2\dot{y}_0 + 8\bar{m}\bar{n}^2\dot{x}_0 \cos(\bar{n}(2\Delta t + t^*)) \\
&\quad - 8\bar{m}\bar{n}^3x_0 \sin(\bar{n}(2\Delta t + t^*)) + 32\bar{m}^3\bar{n}x_0 \sin(\bar{n}(2\Delta t + t^*)) \\
&\quad \left. + 16\bar{m}^2\bar{n}\dot{y}_0 \sin(\bar{n}(2\Delta t + t^*)) - 32\bar{m}^3\bar{n}^2t^*x_0 - 16\bar{m}^2\bar{n}^2t^*\dot{y}_0 \right] \\
\dot{x}_f &= \frac{1}{4\bar{n}^2} \left[ 2\bar{m}\bar{u}_y + 4\bar{n}^2\dot{x}_0 \cos(\bar{n}(2\Delta t + t^*)) - 4\bar{n}^3x_0 \sin(\bar{n}(2\Delta t + t^*)) \right. \\
&\quad + 4\bar{m}\bar{u}_y \cos(\bar{n}(\Delta t + t^*)) - 2\bar{n}\bar{u}_x \sin(\bar{n}(\Delta t + t^*)) + 4\bar{m}\bar{u}_y \cos(\bar{n}\Delta t) \\
&\quad + 2\bar{m}\bar{u}_y \cos(2\bar{n}\Delta t) - 2\bar{n}\bar{u}_x \sin(\bar{n}\Delta t) - \bar{n}\bar{u}_x \sin(2\bar{n}\Delta t) + 2\bar{m}\bar{u}_y \cos(\bar{n}t^*) \\
&\quad - 4\bar{m}\bar{u}_y \cos(\bar{n}t^*/2) + 2\bar{m}\bar{u}_y \cos(\bar{n}(2\Delta t + t^*)) \\
&\quad - 8\bar{m}\bar{u}_y \cos(\bar{n}(2\Delta t + t^*)/2) - 4\bar{m}\bar{u}_y \cos(\bar{n}(4\Delta t + t^*)/2) - \bar{n}\bar{u}_x \sin(\bar{n}t^*) \\
&\quad + 2\bar{n}\bar{u}_x \sin(\bar{n}t^*/2) - \bar{n}\bar{u}_x \sin(\bar{n}(2\Delta t + t^*)) + 4\bar{n}\bar{u}_x \sin(\bar{n}(2\Delta t + t^*)/2) \\
&\quad + 2\bar{n}\bar{u}_x \sin(\bar{n}(4\Delta t + t^*)/2) + 8\bar{m}\bar{n}\dot{y}_0 \sin(\bar{n}(2\Delta t + t^*)) \\
&\quad \left. + 16\bar{m}^2\bar{n}x_0 \sin(\bar{n}(2\Delta t + t^*)) \right] \\
\dot{y}_f &= -\frac{1}{2\bar{n}^3} \left[ 16\bar{m}^3\bar{n}x_0 - 4\bar{m}\bar{n}^3x_0 - 2\bar{n}^3\dot{y}_0 + 8\bar{m}^2\bar{n}\dot{y}_0 + 4\bar{m}^2\bar{u}_y \sin(\bar{n}\Delta t) \right. \\
&\quad + 2\bar{m}^2\bar{u}_y \sin(2\bar{n}\Delta t) + 2\bar{m}^2\bar{u}_y \sin(\bar{n}t^*) - 4\bar{m}^2\bar{u}_y \sin(\bar{n}t^*/2) \\
&\quad + 2\bar{m}^2\bar{u}_y \sin(\bar{n}(2\Delta t + t^*)) - 8\bar{m}^2\bar{u}_y \sin(\bar{n}(2\Delta t + t^*)/2) \\
&\quad - 4\bar{m}^2\bar{u}_y \sin(\bar{n}(4\Delta t + t^*)/2) + \bar{m}\bar{n}\bar{u}_x + 4\bar{m}^2\bar{u}_y \sin(\bar{n}(\Delta t + t^*)) \\
&\quad + 2\bar{m}\bar{n}\bar{u}_x \cos(\bar{n}\Delta t) + \bar{m}\bar{n}\bar{u}_x \cos(2\bar{n}\Delta t) + \bar{m}\bar{n}\bar{u}_x \cos(\bar{n}t^*) \\
&\quad - 2\bar{m}\bar{n}\bar{u}_x \cos(\bar{n}t^*/2) + \bar{m}\bar{n}\bar{u}_x \cos(\bar{n}(2\Delta t + t^*)) \\
&\quad - 4\bar{m}\bar{n}\bar{u}_x \cos(\bar{n}(2\Delta t + t^*)/2) - 2\bar{m}\bar{n}\bar{u}_x \cos(\bar{n}(4\Delta t + t^*)/2) \\
&\quad + 4\bar{m}\bar{n}^3x_0 \cos(\bar{n}(2\Delta t + t^*)) - 16\bar{m}^3\bar{n}x_0 \cos(\bar{n}(2\Delta t + t^*)) \\
&\quad - 8\bar{m}^2\bar{n}\dot{y}_0 \cos(\bar{n}(2\Delta t + t^*)) + 4\bar{m}\bar{n}^2\dot{x}_0 \sin(\bar{n}(2\Delta t + t^*)) \\
&\quad \left. + 2\bar{m}\bar{n}\bar{u}_x \cos(\bar{n}(\Delta t + t^*)) \right] \\
\bar{u}_x &= \bar{u} \sin \alpha \\
\bar{u}_y &= \bar{u} \cos \alpha
\end{aligned} \tag{29}$$

APPENDIX C: ZV FINAL RELATIVE ECCENTRICITY

$$e_{rel} = \sqrt{\frac{1}{4\bar{m}^2\bar{n}^6} \left[ \begin{aligned} &8\bar{m}^3\bar{n}x_0 - 8\bar{m}\bar{n}^3x_0 - 4\bar{n}^3\dot{y}_0 + 4\bar{m}^2\bar{n}\dot{y}_0 + 2\bar{m}^2\bar{u}_y \sin(\Delta t\bar{n}) \\ &+ 2\bar{m}^2\bar{u}_y \sin(\bar{n}t^*) - 4\bar{m}^2\bar{u}_y D - 4\bar{m}^2\bar{u}_y \sin(C) + \bar{m}\bar{n}\bar{u}_x \\ &+ 2\bar{m}^2\bar{u}_y A + \bar{m}\bar{n}\bar{u}_x \cos(\Delta t\bar{n}) + \bar{m}\bar{n}\bar{u}_x \cos(\bar{n}t^*) - 2\bar{m}\bar{n}\bar{u}_x E \\ &- 2\bar{m}\bar{n}\bar{u}_x \cos(C) + 2\bar{m}\bar{n}^3x_0 B - 8\bar{m}^3\bar{n}x_0 B - 4\bar{m}^2\bar{n}\dot{y}_0 B \\ &+ 2\bar{m}\bar{n}^2\dot{x}_0 A + \bar{m}\bar{n}\bar{u}_x B \end{aligned} \right]^2 + \frac{\bar{m}^2}{\bar{n}^8} \left[ \begin{aligned} &2\bar{m}\bar{u}_y + 2\bar{m}\bar{u}_y B - \bar{n}\bar{u}_x A + 2\bar{m}\bar{u}_y \cos(\Delta t\bar{n}) - \bar{n}\bar{u}_x \sin(\Delta t\bar{n}) \\ &+ 2\bar{m}\bar{u}_y \cos(\bar{n}t^*) - 4\bar{m}\bar{u}_y E - 4\bar{m}\bar{u}_y \cos(C) + 2\bar{n}^2\dot{x}_0 B \\ &- \bar{n}\bar{u}_x \sin(\bar{n}t^*) + 2\bar{n}\bar{u}_x D + 2\bar{n}\bar{u}_x \sin(C) - 2\bar{n}^3x_0 A \\ &+ 4\bar{m}\bar{n}\dot{y}_0 A + 8\bar{m}^2\bar{n}x_0 A \end{aligned} \right]^2}$$

where

$$A = \sin(\bar{n}(\Delta t + t^*))$$

$$B = \cos(\bar{n}(\Delta t + t^*))$$

$$C = \frac{\bar{n}(2\Delta t + t^*)}{2}$$

$$D = \sin\left(\frac{\bar{n}t^*}{2}\right)$$

$$E = \cos\left(\frac{\bar{n}t^*}{2}\right)$$

$$\bar{u}_x = \bar{u} \sin \alpha$$

$$\bar{u}_y = \bar{u} \cos \alpha$$

(30)

**APPENDIX D: ZVD FINAL RELATIVE ECCENTRICITY**

$$e_{rel} = \sqrt{\frac{1}{4\bar{n}^8} \left[ \begin{aligned} &2\bar{m}^2\bar{u}_y + 4\bar{m}^2\bar{u}_y \cos(\Delta t\bar{n}) + 2\bar{m}^2\bar{u}_y D + 2\bar{m}^2\bar{u}_y \cos(\bar{n}t^*) \\ &- 4\bar{m}^2\bar{u}_y F + 2\bar{m}^2\bar{u}_y \cos(A) - 8\bar{m}^2\bar{u}_y \cos(A/2) \\ &- \bar{m}\bar{n}\bar{u}_x C - \bar{m}\bar{n}\bar{u}_x \sin(\bar{n}t^*) + 2\bar{m}\bar{n}\bar{u}_x E - \bar{m}\bar{n}\bar{u}_x \sin(A) \\ &+ 4\bar{m}\bar{n}\bar{u}_x \sin(A/2) + 2\bar{m}\bar{n}\bar{u}_x \sin(B) + 4\bar{m}\bar{n}^2\dot{x}_0 \cos(A) \\ &- 4\bar{m}\bar{n}^3x_0 \sin(A) + 16\bar{m}^3\bar{n}x_0 \sin(A) + 8\bar{m}^2\bar{n}\dot{y}_0 \sin(A) \end{aligned} \right]^2 + \frac{1}{16\bar{m}^2\bar{n}^6} \left[ \begin{aligned} &16\bar{m}^3\bar{n}x_0 - 16\bar{m}\bar{n}^3x_0 - 8\bar{n}^3\dot{y}_0 + 8\bar{m}^2\bar{n}\dot{y}_0 + 4\bar{m}^2\bar{u}_y \sin(\Delta t\bar{n}) \\ &+ 2\bar{m}^2\bar{u}_y C + 2\bar{m}^2\bar{u}_y \sin(\bar{n}t^*) - 4\bar{m}^2\bar{u}_y E + 2\bar{m}^2\bar{u}_y \sin(A) \\ &- 8\bar{m}^2\bar{u}_y \sin(A/2) - 4\bar{m}^2\bar{u}_y \sin(B) + \bar{m}\bar{n}\bar{u}_x + 4\bar{m}^2\bar{u}_y G \\ &+ 2\bar{m}\bar{n}\bar{u}_x \cos(\Delta t\bar{n}) + \bar{m}\bar{n}\bar{u}_x D + \bar{m}\bar{n}\bar{u}_x \cos(\bar{n}t^*) - 2\bar{m}\bar{n}\bar{u}_x F \\ &+ \bar{m}\bar{n}\bar{u}_x \cos(A) - 4\bar{m}\bar{n}\bar{u}_x \cos(A/2) - 2\bar{m}\bar{n}\bar{u}_x \cos(B) \\ &+ 4\bar{m}\bar{n}^3x_0 \cos(A) - 16\bar{m}^3\bar{n}x_0 \cos(A) - 8\bar{m}^2\bar{n}\dot{y}_0 \cos(A) \\ &+ 4\bar{m}\bar{n}^2\dot{x}_0 \sin(A) + 2\bar{m}\bar{n}\bar{u}_x H \end{aligned} \right]^2} \quad (31)$$

where

$$\begin{aligned} A &= \bar{n}(2\Delta t + t^*) \\ B &= \frac{\bar{n}(4\Delta t + t^*)}{2} \\ C &= \sin(2\bar{n}\Delta t) \\ D &= \cos(2\bar{n}\Delta t) \\ E &= \sin(\bar{n}t^*/2) \\ F &= \cos(\bar{n}t^*/2) \\ G &= \sin(\bar{n}(\Delta t + t^*)) \\ H &= \cos(\bar{n}(\Delta t + t^*)) \\ \bar{u}_x &= \bar{u} \sin \alpha \\ \bar{u}_y &= \bar{u} \cos \alpha \end{aligned}$$

## REFERENCES

- <sup>1</sup> Bandyopadhyay, S., Subramanian, G., Foust, R., Morgan, D., Chung, S., and Hadaegh, F., "A Review of Impending Small Satellite Formation Flying Missions," *Proceedings of the 53rd AIAA Aerospace Sciences Meeting*, AIAA, Kissimmee, FL, 2015, pp. 1-17. doi: 10.2514/6.2015-1623
- <sup>2</sup> Agasid, E., *et al.*, "Small Spacecraft Technology State of the Art." NASA Report NASA/TP-2015-216648/REV1, NASA Ames Research Center, Mission Design Division, 2015.
- <sup>3</sup> Buchen, E., "SpaceWorks' 2014 Nano/Microsatellite Market Assessment." *Proceedings of the 28th Annual AIAA/USU Conference on Small Satellites*, AIAA, Logan, UT, 2014, pp. 1-5.
- <sup>4</sup> Singh, T., *Optimal Reference Signal for Dynamical Systems: Theory and Application*," 1<sup>st</sup> ed., CRC Press, Boca Raton, FL, 2010.
- <sup>5</sup> Bevilacqua, R., "Analytical Guidance Solutions for Spacecraft Planar Rephasing via Input Shaping", *Journal of Guidance, Control, and Dynamics*, published online 20 Feb. 2014, Vol. 37, No. 3, 2014, pp. 1042-1047. doi: 10.2514/1.G000008
- <sup>6</sup> Bevilacqua, R., and Lovell, T. A., "Analytical Guidance for Spacecraft Relative Motion Under Constant Thrust using Relative Orbital Elements," *Acta Astronautica*, published online 15 May 2014, Vol. 102, 2014, pp. 47-61. doi: 10.1016/j.actaastro.2014.05.004
- <sup>7</sup> Schweighart, S., and Sedwick, R., "A Perturbative Analysis of Geopotential Disturbances for Satellite Cluster Formation Flying", *Proceedings of the 2001 IEEE Aerospace Conference*, IEEE, Big Sky, MT, 2001, Vol. 2, pp. 1001-1019. doi: 10.1109/AERO.2001.931281
- <sup>8</sup> Schweighart, S. A., and Sedwick, R. J. "High-Fidelity Linearized J Model for Satellite Formation Flight", *Journal of Guidance, Control, and Dynamics*, Vol. 25, No. 6, 2002, pp. 1073-1080. doi: 10.2514/2.4986
- <sup>9</sup> Arolovich, I., and Agranovich, G., "Control Improvement of Under-Damped Systems and Structures by Input Shaping", *Proceedings of The 8th Int. Conf. on Material Technologies and Modeling (MMT-2014)*, Ariel, Israel, 2014, Vol. 3, pp. 1-10.
- <sup>10</sup> Singhose, W., Singer, N., and Seering, W., "Comparison of Command Shaping Methods for Reducing Residual Vibration", *Proceedings of the 1995 European Control Conference*, Rome, Italy, 1995.
- <sup>11</sup> Leonard, C. L., Hollister, W. M., and Bergmann, E. V., "Orbital Formationkeeping with Differential Drag", *Journal of Guidance, Control, and Dynamics*, Vol. 12, No. 1. 1989, pp. 108-113. doi: 10.2514/3.20374
- <sup>12</sup> Clohessy, W. H., and Wiltshire, R. S., "Terminal Guidance System for Satellite Rendezvous," *Journal of the Aerospace Sciences*, Vol. 27, No. 9, 1960, pp. 653-658. doi: 10.2514/8.8704